# Realization of linearly polarized exciton emission in wurtzite zinc oxide quantum dots

Zaiping Zeng,[1,*] Christos S. Garoufalis,[2] Sotirios Baskoutas,[2,†] Yu Jia,[1,3,‡] and Gabriel Bester[4,§]

[1]*Key Laboratory for Special Functional Materials of Ministry of Education, Collaborative Innovation Center of Nano Functional Materials and Applications, and School of Materials Science and Engineering, Henan University, Kaifeng, Henan 475001, China*

[2]*Materials Science Department, University of Patras, 26504 Patras, Greece*

[3]*International Laboratory for Quantum Functional Materials of Henan, and School of Physics and Engineering, Zhengzhou University, Zhengzhou, Henan 450001, China*

[4]*Institut für Physikalische Chemie, Universität Hamburg, Grindelallee 117, 20146 Hamburg, Germany*

(Received 24 September 2018; published 6 December 2018)

Linearly polarized exciton emission from a quantum dot is very appealing for polarized light emitting diodes and quantum information science and technologies. However, it has been very difficult to access it, because conventional wurtzite quantum dots (QDs) usually favor circularly polarized exciton emission originating from a single electron bound to a hole with dominant heavy hole ($A$ band) character. Here we explore the exciton fine structure of wurtzite ZnO QDs by means of plane-wave million-atom atomistic pseudopotential calculations and a configuration interaction approach. We demonstrate that linearly polarized emission could be realized in these QDs by (i) enhancing the quantum confinement effects and (ii) applying hydrostatic pressure. Such an exciton has a polarization exclusively along the $c$-axis direction of the QDs, which derives from a single electron bounded to a hole state with a split-off hole ($C$-band) character. This work paves the way for the exploration of the fundamental properties of wurtzite ZnO QDs and their potential applications in optoelectronic devices and quantum technologies.

DOI: 10.1103/PhysRevB.98.235410

## I. INTRODUCTION

Semiconductor quantum dots (QDs) have demonstrated their viable role in current optoelectronic devices and have shown a great promise as a light source for quantum information processes. Incorporation of QDs ensembles in the optically active layers greatly improves the color saturation and device efficiencies of laser diodes and QD-based light emitting diodes, which have great potential in the next generation of display and solid-state lighting [1,2]. The proposed quantum computer applications rely on photons with distinct energy and polarization vectors, which can be seen as the ultimate demand on photons emitted from individual QDs [3]. A common requirement raised for several optoelectronic applications, e.g., liquid-crystal displays, three-dimensional visualization, (bio)dermatology [4], optical quantum computers [5], and quantum cryptography [6], is the need of linearly polarized light for their operation. For existing operations, the generation of linearly polarized light is obtained by passing unpolarized light through a combination of polarization selective filters and waveguides, accompanied by an inevitable efficiency loss. These losses can be drastically reduced by employment of light sources, which directly generate photons with desired polarization direction.

Zinc oxide (ZnO), a typical group II-VI compound with wurtzite structure, has a band gap close to GaN. First-principles calculations [7] and magneto-optical measurements [8,9] have brought deep insight into the valence-band ordering and excitonic structure in bulk ZnO. Two important characteristics are revealed [cf. Fig. 1(a)]: (i) crystal field, which is a common feature for wurtzite structure, splits the $\Gamma_{1v}$ band into a twofold $\Gamma_{1v}$ band and a fourfold $\Gamma_{5v}$ band; (ii) "negative" spin-orbit splitting, which is rather unique for ZnO, splits the fourfold $\Gamma_{5v}$ band into $\Gamma_{7v}$ and $\Gamma_{9v}$ bands. Both of them are twofold and the former band lies unusually above the latter one. The incorporation of the spin-orbit interaction also translates the $\Gamma_{1v}$ band to the $\Gamma_{7v}$ band. These three valence bands from top to bottom, $\Gamma_{7v}$, $\Gamma_{9v}$, $\Gamma_{7v}$, are the so-called A (heavy hole), B (light hole), and C (split-off hole) bands, respectively. Bulk ZnO material belongs to the $C_{6v}^4$ point group. Consequently, the highest point-group symmetry for colloidal ZnO QDs is $C_{3v}$, having a threefold rotation axis along its growth direction (i.e., [0001] crystallographic direction). In this contribution, we report that linearly polarized exciton emission could be realized in these high-symmetry ZnO QDs by (i) enhancing quantum confinement and (ii) applying hydrostatic pressure.

## II. COMPUTATIONAL DETAILS

We consider oxygen-centered ZnO QDs within the strong and intermediate quantum confinement regime with sizes (diameter $D = 1.7$ and 3.6 nm) which can be easily achieved experimentally via the well-established colloidal fabrication method (e.g., cf. Ref. [10]). The interatomic distances are

*zaiping.zeng@henu.edu.cn
†bask@upatras.gr
‡jiayu@henu.edu.cn
§gabriel.bester@uni-hamburg.de

 

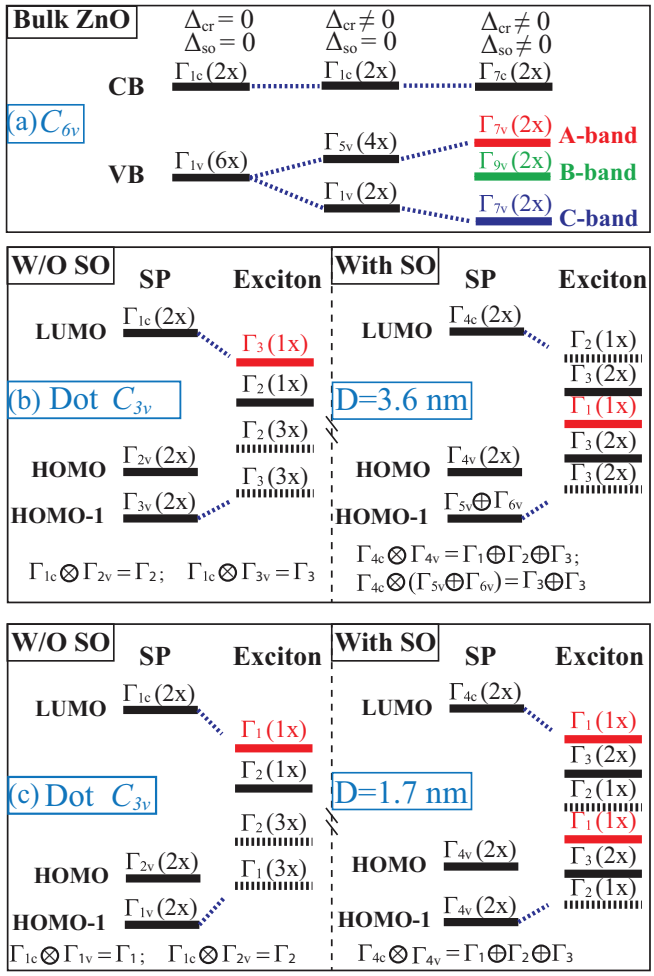


FIG. 1. (a) Symmetry evolution of the conduction-band minimum (CBM) and valence band maximum (VBM) with including crystal field ($\Delta_{cr}$) and/or spin-orbit interaction ($\Delta_{so}$) in bulk ZnO with point group symmetry $C_{6v}$. Symmetry analysis of ZnO quantum dots (i.e., $C_{3v}$ point group symmetry) with diameter (b) $D = 3.6$ nm and (c) 1.7 nm both without and with spin-orbit interaction. The left column of each sub-panel gives the symmetry of the lowest unoccupied molecular orbital (LUMO) and first two highest occupied molecular orbital (HOMO) states. The right column gives the resulting excitons with their corresponding point-group symmetries. A thick black dashed line indicates an optically dark state, and a solid black (red) line indicates an in-plane (out-of-plane) polarized optically bright state. The degeneracy of the corresponding energy levels is shown in the parentheses. We employ Koster's notation for both the single and double group symmetry representations.

taken as the experimental bulk values, which naturally leads to a $C_{3v}$ symmetry for spherical colloidal QDs, characterized solely by their diameter $D$. The dangling bonds at the surface of the QDs are passivated by a high-band-gap artificial material, as successfully practiced previously [11]. The single-particle calculations are based on the atomistic empirical pseudopotential method using well-tested pseudopotentials [12], taking strain, band coupling, coupling between different parts of the Brillouin zone, and spin-orbit coupling into account. The correlated excitonic states are calculated by the configuration interaction approach using all possible singly excited determinants constructed from the 12 lowest (highest) energy electron (hole) states, thus taking correlations into account. The Coulomb and exchange integrals are calculated from the atomic wave functions and are screened by the phenomenological microscopic, isotropic, and uniform model proposed by Resta [13]. The optical dipole matrix elements are calculated within the dipole approximation, and the oscillator strength is calculated via Fermi's "golden rule."

## III. RESULTS AND DISCUSSION

We start the exploration from a high-symmetry ZnO QD in the regime of intermediate quantum confinement (e.g., $D = 3.6$ nm). The corresponding electronic structure and band-edge exciton fine structure are shown in Fig. 1(b). In the absence of spin-orbit and exchange interactions, the electron-hole pair is always fourfold degenerate (not shown). This fourfold manifold is split into a threefold triplet state and a onefold singlet state when exchange interaction is switched on. The triplet state is spin forbidden, being optically dark and energetically lower, while the singlet state is spin allowed, being optically bright and energetically higher. The singlet-triplet splitting is around 11.3 meV [i.e., energy difference between the $\Gamma_3$ states in the left panel of Fig. 1(b)]. We found that the first dark exciton state has $\Gamma_3$ symmetry and originates from the HOMO-1 $\rightarrow$ LUMO transition, where the HOMO-1 and LUMO states belong to the $\Gamma_{3v}$ and $\Gamma_{1c}$ representations, respectively. The first bright exciton state exhibits $\Gamma_2$ symmetry, stemming from the HOMO $\rightarrow$ LUMO transition, where the HOMO and LUMO states have $\Gamma_{2v}$ and $\Gamma_{1c}$ symmetries, respectively. When the spin-orbit interaction is included, the LUMO state is found to have $\Gamma_{4c}$ symmetry, while the HOMO and HOMO-1 states have $\Gamma_{4c}$ and $\Gamma_{5v}\bigoplus\Gamma_{6v}$ symmetries, respectively. To further elucidate the electronic structure, we project the fast oscillating atomic wave functions onto the bulk Bloch states. This gives us access to the envelope functions, which is more convenient to visualize. It appears that the LUMO state has a $S$-type envelope function and has a dominant contribution from the lowest $\Gamma_{7c}$ conduction band (cf. Fig. 2). However, the HOMO state, which has an equal contribution from bulk $A$ and $B$ bands, exhibits a $P_{xy}$-type orbital character. The neighboring hole states, namely HOMO-1 and HOMO-2 states, have a dominant contribution from bulk $A$-band and $B$-band, respectively [cf. second column of Fig. 2 (rows 3 and 4)]. As mentioned previously (Fig. 1), we find that the HOMO $\rightarrow$ LUMO transition does not lead to the formation of the ground-state exciton manifold. On the contrary, the transition from the HOMO-1 state to the LUMO state forms the ground-state exciton manifold. This surprising phenomenon is attributed to the different Coulomb interaction between the electron and hole states having the same $S$-type orbital (larger) compared to electron state with $S$-type orbital and the hole state with $P_{xy}$-type orbital (smaller). A larger (negative) Coulomb interaction therefore drags the exciton manifold formed from the HOMO-1 $\rightarrow$ LUMO transition down to the ground state [cf. Fig. 1(b)].

According to the group theory analysis, the exciton symmetry can be obtained as the direct product of the single-particle electron and hole state involved in the transition. We find that the exciton manifold ensuring from the

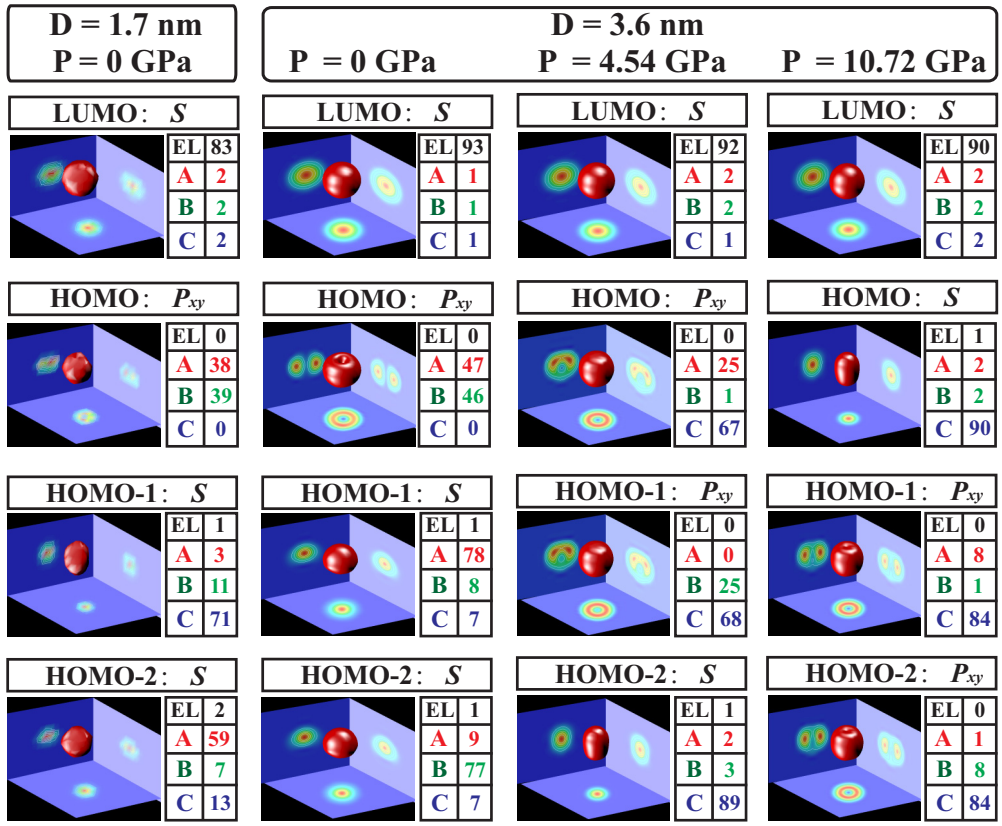


FIG. 2. Envelope functions for the electron (LUMO) and first three hole states (HOMO, HOMO-1, HOMO-2) for high-symmetry ZnO quantum dots with diameter $D = 1.7$ nm and with $D = 3.6$ nm under various pressures. The isosurfaces enclose 75% of the state densities. To trace the parentage of each dot state for analysis purpose, the real atomistic dot wave function is projected on the top three valence-band states (labeled as A, B, and C) and the lowest conduction-band state (labeled as El). We use the notation $\omega_\zeta$ to describe the symmetry of the envelope functions, where $\omega$ donates the number of nodes encountered by moving across the in-plane ($xy$ direction) or out-of-plane ($z$ direction) directions, and $\zeta$ represents the direction in which we find the node(s). The number of nodes can be easily counted on the three projected planes. The possible values for $\omega$ are $S$, $P$, etc., where $S$ indicates the form of the envelope function without a node (in this case, we neglect the subscript $\zeta$), $P$ with one node, etc. The obtained Bloch function characters and envelope function character for each state are presented beside and above each plot, respectively.

HOMO $\rightarrow$ LUMO transition consists of a singly degenerate, out-of-plane polarized bright state with $\Gamma_1$ symmetry being energetically lower, a singly degenerate dark state with $\Gamma_2$ symmetry being energetically higher, and a doubly degenerate in-plane polarized state with $\Gamma_3$ symmetry in between. The ground-state exciton manifold is found to be formed from HOMO-1 $\rightarrow$ LUMO transition, which gives a twofold dark state with $\Gamma_3^*$ symmetry at a lower energy and a twofold, in-plane polarized bright state with $\Gamma_3$ symmetry at a higher energy. This doubly degenerate $\Gamma_3$ bright exciton state gives rise to a vanishing fine-structure splitting (FSS), therefore making these high-symmetry ZnO QDs as ideal sources of entangled photon pairs. A similar proposal has been suggested for [111]-grown epitaxial zinc-blende QDs and heterostructure quantum wires [14,15], and has been experimentally realized by fabricating QDs on a high-symmetry crystallographic (111) substrate [16]. Nearly dephasing-free polarization entangled photon pairs generated from a zinc-blende quantum dot utilizing strain has been experimentally demonstrated very recently [17]. As aforementioned, only ideal high-symmetry ($C_{3v}$) ZnO QDs with nearly spherical shape are considered in this work. Any change in the shape or the presence of impurity on the surface would lead to the lowering of the atomistic symmetry of the quantum dot from $C_{3v}$ symmetry, which in turn will cause the splitting of the twofold $\Gamma_3$ states and therefore the presence of FSS. Although being optically active, the $\Gamma_1$ state exhibits an oscillator strength a few orders of magnitude weaker than the ground-state, in-plane polarized $\Gamma_3$ state, and is therefore nearly optically dark. The corresponding photoluminescence spectra exhibits a circularly polarized band-edge emission as a result [cf. Figs. 3(c) and 3(d)].

When the QD is brought into the strong quantum confinement regime (i.e., $D = 1.7$ nm), we find that in the absence of spin-orbit interaction, the HOMO and LUMO states remain $\Gamma_{2v}$ and $\Gamma_{1c}$ symmetries, respectively [cf. Fig. 1(c)]. However, due to the increase in the quantum confinement, the HOMO-1 state switches from a $\Gamma_{3v}$ symmetry to a $\Gamma_{1v}$ symmetry. This results in a threefold spin-triplet exciton state with $\Gamma_1$ symmetry being the ground state. When the spin-orbit interaction is included [cf. the right subpanel of Fig. 1(c)], the LUMO state keeps the $S$-type orbital character and its bulk origin (e.g., the $\Gamma_{7c}$ conduction band; cf. Fig. 1). The HOMO state remains $P_{xy}$-type orbital and mainly derives from an equal contribution of bulk $A$ and $B$ bands. Strikingly, the hole state (e.g., HOMO-1) with a dominant $C$-band contribution rises above

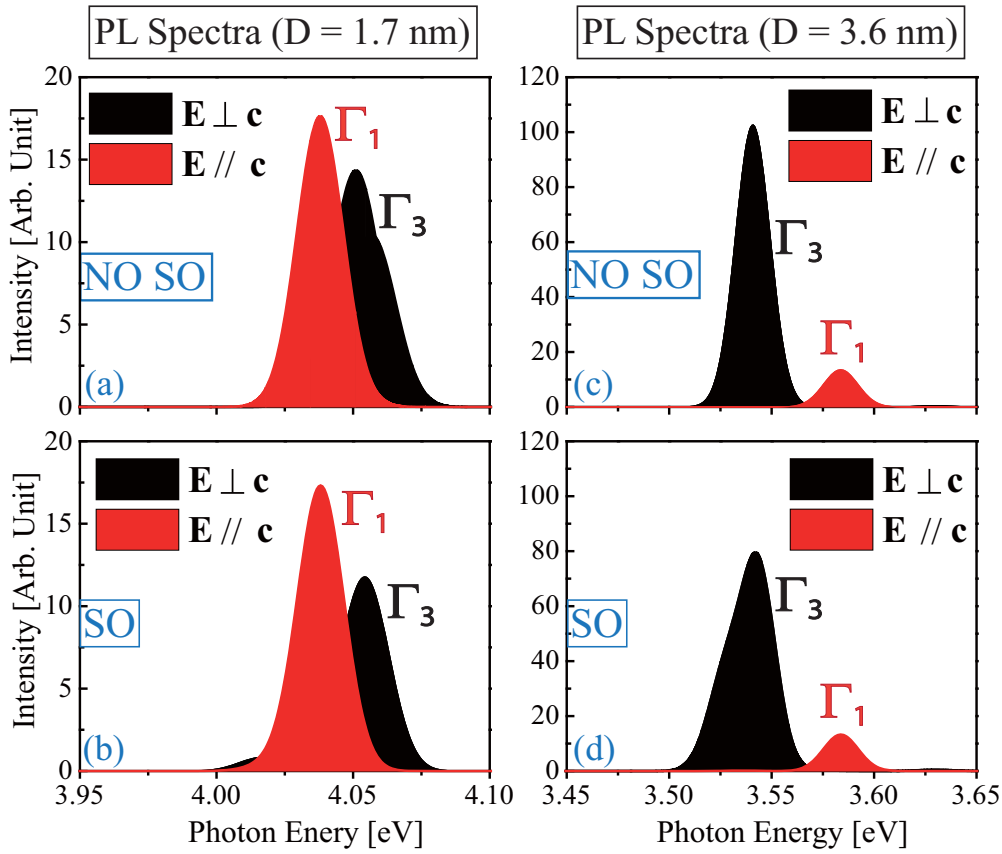


FIG. 3. Simulated photoluminescence spectra of ZnO quantum dots with diameter (a), (b) $D = 1.7$ nm and (c), (d) 3.6 nm, (a), (c) excluding or (b), (d) including spin-orbit interaction. A Gaussian broadening function is employed with a linewidth $\Gamma_g = 10$ meV. In-plane polarized exciton emission ($\vec{E} \perp \vec{c}$) is shown in black curve, and that along the out-of-plane direction ($\vec{E} \parallel \vec{c}$) is shown in red curve. The symmetry of the exciton state is indicated alongside the emitting peak.

that with a dominant $A$-band counterpart (e.g., HOMO-2) and becomes energetically more favorable. This is attributed to the nontrivial interplay between the symmetry mixing, spin-orbit coupling, and quantum confinement effects on the QD valence-band electronic structure. A similar behavior has also been found in InN nanowires explored by first-principles calculations based on many-body perturbation theory [18]. Such a reordering in the hole states causes a drastic change in the band-edge exciton symmetry as shown in Fig. 1(c). The HOMO-1 $\rightarrow$ LUMO transition again forms the ground-state exciton manifold but consists of a singly degenerate, optically inactive state with $\Gamma_2$ symmetry at a lower energy, a singly degenerate, optically active and out-of-plane polarized state with $\Gamma_1$ symmetry at a higher energy, and a doubly degenerate, in-plane polarized state with $\Gamma_3$ symmetry in between [cf. Fig. 1(c)]. We find that the $\Gamma_2$ and $\Gamma_3$ exciton states are closer in energy (e.g., 20 $\mu$eV) and $\Gamma_1$ state is significantly far away ($E_X^{\Gamma_1} - E_X^{\Gamma_2} = 0.03$ meV). Concerning the emission intensity, the oscillator strength of the $\Gamma_3$ exciton is four orders of magnitude weaker than that of its $\Gamma_1$ counterpart. Consequently, the corresponding photoluminescence spectra exhibit a band-edge emission exclusively along the $c$ axis of the QD [cf. Figs. 3(a) and 3(c)]. We note that the temperature effect is not considered throughout the work. In general, it should have profound effects on the exciton fine structure, as has already been found in bulk ZnO [19]. The states with energy splittings in the energy range of a few tens of microelectron volts are likely to be overlapped in a room-temperature environment.

As shown above, ZnO QDs within the intermediate quantum confinement regime exhibits a circularly polarized exciton emission. In an attempt to possibly manipulate its emission polarization to reach finally linearly polarized light emission, we apply hydrostatic pressure in these QDs. The pressure is created by equally compressing the lattice constants in both the in-plane and out-of-plane directions. The pressure values are obtained approximately by using the Murnaghan equation of state [20,21], $P = (B/B')[(V_0/V)^{B'} - 1]$, where $V_0$ and $V$ are the volumes without and with applied pressure, respectively, taking the bulk modulus of ZnO $B = 142.4$ GPa and the pressure derivative of the bulk modulus $B' = 3.6$ [22]. To fully capture the pressure effect, our screened atomic pseudopotentials $v_\alpha$ (with $\alpha =$ Zn, O) incorporate the dependence on the local hydrostatic strain Tr($\epsilon$) through the relation [21] $v_\alpha(r, \epsilon) = v_\alpha^{eq}(r; 0)[1 + \gamma_\alpha \mathrm{Tr}(\epsilon)]$, where $v_\alpha^{eq}$ is the pseudopotential at zero pressure and $\gamma_\alpha$ is a fitting parameter. In our calculations, $\gamma_\alpha$ is taken as 0.304 which gives the pressure coefficient for bulk ZnO equal to 24.7 meV/GPa, reproducing exactly the experimental value $24.7 \pm 0.1$ meV/GPa [22]. For each applied pressure, the atomic positions for the dot atoms are relaxed to the minimum strain energy using

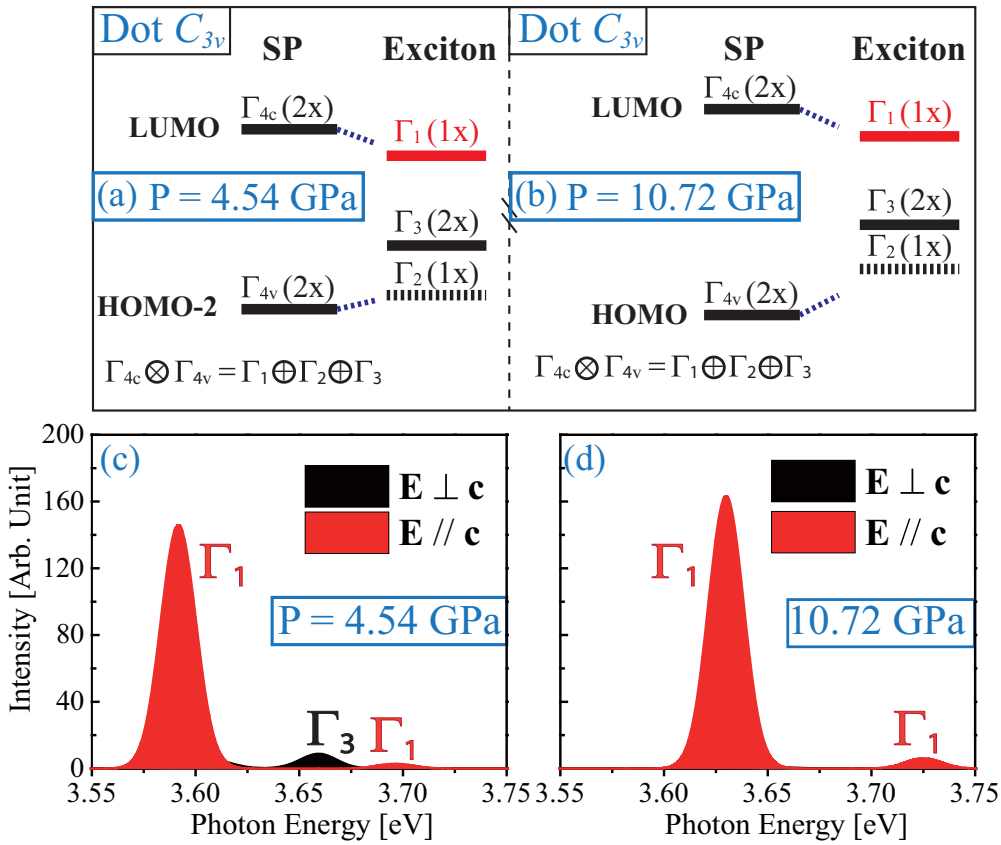


FIG. 4. (a), (b) Symmetry analysis of ZnO quantum dots (i.e., $C_{3v}$ point-group symmetry) with diameter $D = 3.6$ nm under hydrostatic pressure (a) $P = 4.52$ GPa and (b) 10.72 GPa, respectively, considering the spin-orbit interaction. The left column of each subpanel gives the symmetry of the electron and hole states involved in the formation of the band-edge exciton manyfold. The right column gives the resulting band-edge excitons with their corresponding point-group symmetries. A thick black dashed line indicates an optically dark state, and a solid black (red) line indicates an in-plane (out-of-plane) polarized optically bright state. The degeneracy of the corresponding energy levels is shown in the parentheses. (c), (d) Simulated photoluminescence spectrum of ZnO quantum dots with diameter $D = 3.6$ nm under pressure (c) $P = 4.54$ and (d) 10.72 GPa, respectively. A Gaussian broadening function is employed with a linewidth $\Gamma_g = 10$ meV. In-plane polarized exciton emission ($\vec{E} \perp \vec{c}$) is shown in black curve, and that along the out-of-plane direction ($\vec{E} \parallel \vec{c}$) is shown in red curve. The symmetry of the exciton state is indicated alongside the emitting peak.

Keating's valence force field (VFF) model for wurtzite materials [23]. As the VFF input parameters, the two bond-stretching constants ($\alpha$ and $\alpha'$) and two bond-bending constants ($\beta$ and $\beta'$) are taken as $\alpha = 59.15$ N/m, $\alpha' = 80.23$ N/m, $\beta = 6.88$ N/m, and $\beta' = 7.63$ N/m, respectively. The resultant elastic constants ($C_{ij}$) and bulk modulus ($B$) are $C_{11} = 209.7$ GPa, $C_{33} = 211.4$ GPa, $C_{12} = 121.8$ GPa, $C_{13} = 103.8$ GPa, $C_{44} = 41.32$ GPa, $C_{66} = 43.9$ GPa, and $B = 143.1$ GPa, respectively, reproducing almost exactly the corresponding experimental values [22,24]: $C_{11} = 209.7$ GPa, $C_{33} = 210.9$ GPa, $C_{12} = 121.1$ GPa, $C_{13} = 105.1$ GPa, $C_{44} = 42.47$ GPa, $C_{66} = 44.3$ GPa, and $B = 142.4$ GPa. After the relaxation, the structure remains the $C_{3v}$ symmetry.

We find that the LUMO state under pressure is purely derived from bulk Bloch $\Gamma_{7c}$ conduction band (∼90%), retaining the same parentage as in the zero-pressure case (cf. Fig. 2), whereas, for the hole states, the applied pressure exhibits two important effects: (i) it increases significantly the bulk Bloch $C$-band contribution to the dot hole states, (ii) it brings the state which mainly (or purely) derives from bulk Bloch $C$ band and presents an $S$-type orbital up to an energetically more favorable position [$h_5$ ($P = 0$) → $h_2$ ($P = 4.54$ GPa) → $h_0$ ($P = 10.72$ GPa)]. These two effects turns out to have a significant effect on the QD band-edge emission. For relatively weak pressures, the hole state with a dominant $A$-band contribution having a $\Gamma_{5v} \bigoplus \Gamma_{6v}$ symmetry is energetically more favorable, which is similar to the zero pressure case. The transition from this hole state to the lowest electron state forms the ground-state exciton manifold, consisting of a twofold $\Gamma_3^*$ dark state and a twofold $\Gamma_3$ in-plane polarized bright exciton states. Thanks to the pressure effects, the hole with a dominant $C$-band contribution and a $S$-type orbital rises up. This is attributed to a smaller deformation of bulk $C$ band compared to that of bulk $A$ and $B$ bands [25]. When the pressure keeps increasing and reaches up to a critical pressure (e.g., $P_c = 4.54$ GPa), an energetically more favorable hole state with pure $C$-band parentage, which combines with the lowest electron state, contributes exclusively to the ground-state exciton manifold. Similar to the QDs in the strong confinement regime, this ground-state manifold produces a $\Gamma_1$ state with emission polarization exclusively along the $c$-axis direction [$\vec{E} \parallel \vec{c}$, cf. Fig. 4(c)]. Further increase

in the pressure causes a blueshift in the emission spectra and a significant enhancement in the linear polarization emission intensity [cf. Fig. 4(d)].

## IV. CONCLUSION

To summarize, we have theoretically resolved the exciton fine structure of high-symmetry wurtzite ZnO quantum dots by employing a million-atoms atomistic empirical pseudopotential method combined with a configuration interaction approach. We find that these high-symmetry QDs in the intermediate quantum confinement regime exhibits a circularly polarized light emission, which mainly originates from a doubly degenerate $\Gamma_3$ exciton formed from an electron state derived from the lowest bulk conduction band and a hole state contributed from the bulk valence *A* band. We have demonstrated that a linearly polarized exciton emission can be effectively activated via (i) enhancing the quantum confinement effects and (ii) applying hydrostatic pressure. The band-edge exciton with polarization solely along the *c*-axis direction have a parentage from a singly degenerate $\Gamma_1$ state stemming from an electron state derived from the lowest bulk conduction band and a hole state contributed nearly purely from the bulk valence *C* band. This work paves the way for the exploration of the fundamental properties of wurtzite ZnO QDs and their potential applications in optoelectronic devices and quantum technologies.

## ACKNOWLEDGMENTS

Z.Z. acknowledges the "Distinguished Professor" starting grant of Henan University with Grant No. 2018001T and NSFC project with Grant No. 11804077 for financial support. Y.J. has been funded by the NSFC project with Grant No. 11774078. This work has also been cofinanced by the European Union [European Social Fund (ESF)] and by Greek national funds through the Operational Program "Education and Lifelong Learning" of the National Strategic Reference Framework (NSRF)-Research Funding Program: Thales, investing in knowledge society through the ESF.

[1] X. Dai, Z. Zhang, Y. Jin, Y. Niu, H. Cao, X. Liang, L. Chen, J. Wang, and X. Peng, Nature (London) **515**, 96 (2014).
[2] X. Li, Y.-B. Zhao, F. Fan, L. Levina, M. Liu, R. Quintero-Bermudez, X. Gong, L. N. Quan, J. Fan, Z. Yang, S. Hoogland, O. Voznyy, Z.-H. Lu, and E. H. Sargent, Nat. Photon. **12**, 159 (2018).
[3] A. J. Shields, Nat. Photon. **1**, 215 (2007).
[4] N. Zeng, X. Jiang, Q. Gao, H. He, and H. Ma, Appl. Opt. **48**, 6734 (2009).
[5] E. Knill, R. Laflamme, and G. J. Milburn, Nature (London) **409**, 46 (2001).
[6] A. Muller, J. Breguet, and N. Gisin, Europhys. Lett. **23**, 383 (1993).
[7] W. R. L. Lambrecht, A. V. Rodina, S. Limpijumnong, B. Segall, and B. K. Meyer, Phys. Rev. B **65**, 075207 (2002).
[8] D. C. Reynolds, D. C. Look, B. Jogai, C. W. Litton, G. Cantwell, and W. C. Harsch, Phys. Rev. B **60**, 2340 (1999).
[9] L. Ding, C. Yang, H. He, J. Wang, Z. Tang, B. A. Foreman, F. Jiang, and W. Ge, New J. Phys. **15**, 033015 (2013).
[10] K.-F. Lin, H.-M. Cheng, H.-C. Hsu, L.-J. Lin, and W.-F. Hsieh, Chem. Phys. Lett. **409**, 208 (2005).
[11] M. Califano, G. Bester, and A. Zunger, Nano Lett. **3**, 1197 (2003).
[12] S. Baskoutas and G. Bester, J. Phys. Chem. C **114**, 9301 (2010).
[13] R. Resta, Phys. Rev. B **16**, 2717 (1977).
[14] R. Singh and G. Bester, Phys. Rev. Lett. **103**, 063601 (2009).
[15] K. F. Karlsson, M. A. Dupertuis, D. Y. Oberli, E. Pelucchi, A. Rudra, P. O. Holtz, and E. Kapon, Phys. Rev. B **81**, 161307 (2010).
[16] T. Kuroda, T. Mano, N. Ha, H. Nakajima, H. Kumano, B. Urbaszek, M. Jo, M. Abbarchi, Y. Sakuma, K. Sakoda, I. Suemune, X. Marie, and T. Amand, Phys. Rev. B **88**, 041306 (2013).
[17] D. Huber, M. Reindl, S. F. Covre da Silva, C. Schimpf, J. Martín-Sánchez, H. Huang, G. Piredda, J. Edlinger, A. Rastelli, and R. Trotta, Phys. Rev. Lett. **121**, 033902 (2018).
[18] D. Bayerl and E. Kioupakis, Nano Lett. **14**, 3709 (2014).
[19] A. Teke, Ü. Özgür, S. Doğan, X. Gu, H. Morkoç, B. Nemeth, J. Nause, and H. O. Everitt, Phys. Rev. B **70**, 195207 (2004).
[20] G. A. Narvaez, G. Bester, and A. Zunger, Phys. Rev. B **72**, 041307 (2005).
[21] A. J. Williamson, L. W. Wang, and A. Zunger, Phys. Rev. B **62**, 12963 (2000).
[22] H. Morkoç and U. Özgür, *Zinc Oxide* (Wiley-VCH, New York, 2009).
[23] D. Camacho and Y. M. Niquet, Physica E (Amsterdam) **42**, 1361 (2010).
[24] T. B. Bateman, J. Appl. Phys. **33**, 3309 (1962).
[25] A. Schleife, C. Rodl, F. Fuchs, J. Furthmuller, and F. Bechstedt, Appl. Phys. Lett. **91**, 241915 (2007).